Analytic Field Propagation TFSF Boundary for FDTD Problems Involving Planar Interfaces: Lossy Material and Evanescent Fields

Kakhkhor Abdijalilov and John B. Schneider, *Member, IEEE*

***Abstract*—Recently, total-field scattered-field (TFSF) boundaries have been developed for the finite-difference time-domain (FDTD) method which are essentially perfect. The implementation requires an analytic description of the incident field and hence is termed the analytic field propagation (AFP) TFSF method. Previous papers described the implementation for problems involving homogeneous as well as layered media. In this work we provide the details for problems involving lossy media. Additionally, the case of fields incident beyond the critical angle are considered (i.e., when, for lossless material, there is total reflection of the incoming wave and the fields in the second medium are evanescent).**

***Index Terms*—Finite-difference time-domain (FDTD) methods.**

I. Introduction

The total-field/scattered-field (TFSF) boundary, first proposed in [1], is a method for introducing incident fields into finite-difference time-domain (FDTD) grids. The TFSF boundary separates FDTD grids into a total-field (TF) and a scattered-field (SF) region. The nodes in the TF region represent the sum of the incident and any scattered field while the nodes in the SF region corresponds to only scattered fields. Nodes tangential to the TFSF boundary will have a neighboring node on the other side of the boundary. To obtain consistent update equations, the incident field will either have to be subtracted from or added to the value of that neighbor. The TFSF boundary requires that one specify the incident field for all nodes tangential to the boundary for all time-steps. An excellent description of the implementation of the TFSF boundary can be found in [2].

Here we build upon the work presented in [3]–[5] which we term the analytic field propagation (AFP) technique. This technique uses the dispersion relation to obtain an analytic description of the fields on the TFSF boundary. The goal is again to model halfspace problems but to introduce loss into the second medium while maintaining the simplicity presented in the previous work. Loss necessitates the use of complex wavenumbers in the second medium. Having made the transition to complex wavenumbers it is a simple matter to consider problems where the incoming field is incident beyond the critical angle, i.e., the fields in the second medium are evanescent.

Manuscript received August 1, 2006; revised September 8, 2006. This work was supported by the Office of Naval Research Code 321OA.

The authors are with the School of Electrical Engineering and Computer Science, Washington State University, Pullman, WA 99164-2752 USA (schneidj@eecs.wsu.edu).

Digital Object Identifier 10.1109/LAWP.2006.885170

II. Lossy Materials

Here we consider a plane wave (identified as the incoming wave) obliquely incident on a lossy halfspace. The incoming wave is assumed to travel in a lossless medium. The boundary between the two media is assumed to be planar insofar as the calculation of the incident field is concerned. For the remainder of this work the term "incident field" implies the sum of the incoming and reflected waves in the lossless medium and the transmitted field in the lossy medium.

The AFP TFSF boundary requires that one calculate analytically the incident field at an arbitrary point. This necessitates calculation of the numeric wavenumbers as well as the numeric reflection and transmission coefficients. We start by describing the equations which govern FDTD propagation in a lossy medium.

Consider a harmonic field polarized in the z direction propagating in the xy plane of an FDTD grid, i.e., TM^z polarization. Using the notation of [4] and [5], the electric and magnetic fields can be written

$$\begin{aligned}\mathbf{a}_z\hat{E}_z &= \mathbf{a}_z\hat{E}_0 e^{-j(\tilde{k}_x m\delta+\tilde{k}_y n\delta)}e^{j\omega q\Delta_t}\\ &= \mathbf{a}_z\hat{E}_0 e^{-j\tilde{\mathbf{k}}\cdot\mathbf{r}}e^{j\omega q\Delta_t} \end{aligned}\tag{1}$$

$$\begin{aligned}\hat{\mathbf{H}} &= \mathbf{a}_x\hat{H}_x+\mathbf{a}_y\hat{H}_y = (\mathbf{a}_x\hat{H}_{0x}+\mathbf{a}_y\hat{H}_{0y})e^{-j\tilde{\mathbf{k}}\cdot\mathbf{r}}e^{j\omega q\Delta_t}\\ &= \hat{\mathbf{H}}_0 e^{-j\tilde{\mathbf{k}}\cdot\mathbf{r}}e^{j\omega q\Delta_t}.\end{aligned}\tag{2}$$

where δ is the spatial step size (assumed uniform), Δ_t is the temporal step size, (m,n) are the spatial indices in the x and y directions, respectively, q is the temporal index, ω is the frequency, $\tilde{\mathbf{k}}=\mathbf{a}_x\tilde{k}_x+\mathbf{a}_y\tilde{k}_y$ is the wave vector, $\mathbf{r}=\mathbf{a}_x m\delta+\mathbf{a}_y n\delta$ is the position vector, and $\hat{E}_0$ is an arbitrary amplitude. A tilde indicates a numeric quantity, i.e., one whose value in the grid differs from that in the continuous world. A hat indicates a quantity is in the frequency domain. The amplitudes $\hat{H}_{0x}$ and $\hat{H}_{0y}$ are dictated by the impedance of the grid.

Discretizing time, Ampere's law expanded about the time-step $q+1/2$ is

$$\nabla\times\mathbf{H}^{q+1/2}=\epsilon\frac{\mathbf{E}^{q+1}-\mathbf{E}^{q}}{\Delta_t}+\sigma\frac{\mathbf{E}^{q+1}+\mathbf{E}^{q}}{2}\tag{3}$$

where the superscript indicates the time step, σ is the conductivity, ϵ is the permittivity, and time-averaging is used to obtain the conduction current at the necessary temporal location. For the given harmonic fields, the temporal finite difference can be expressed as

$$j\frac{2}{\Delta_t a_t}\sin\left(\frac{\omega\Delta_t}{2}\right)\hat{\mathbf{E}}^{q+1/2}=j\Omega\hat{\mathbf{E}}^{q+1/2}\tag{4}$$

whereas the time-average term can be written

$$\cos\left(\frac{\omega\Delta_t}{2}\right)\hat{\mathbf{E}}^{q+1/2} = A\hat{\mathbf{E}}^{q+1/2}. \tag{5}$$

The discretized form of the curl operation is unchanged from that presented in [4], [5]. For a harmonic field, the finite differences in the x and y directions, identified as $\tilde{\partial}_x$ and $\tilde{\partial}_y$, respectively, can be represented by multiplicative operators, i.e.,

$$\tilde{\partial}_\xi = -j\frac{2}{\delta}\sin\left(\frac{\tilde{k}_\xi\delta}{2}\right) = -jK_\xi \tag{6}$$

where $\xi \in \{x, y\}$. Thus, Ampere's law can be written

$$\begin{aligned} -jK_x\hat{H}_{0y} + jK_y\hat{H}_{0x} &= (j\epsilon\Omega + \sigma A)\hat{E}_0 \\ &= j\epsilon\Omega\left[1 - j\frac{\sigma A}{\epsilon\Omega}\right]\hat{E}_0. \end{aligned} \tag{7}$$

The phase term $e^{j\omega(q+1/2)\Delta_t}$ was common to all terms and hence dropped.

Defining $\mathbf{K} = \mathbf{a}_x K_x + \mathbf{a}_y K_y$, the discrete form of Faraday's law can be written

$$-j\mathbf{K}\times\hat{\mathbf{E}}^q = -j\mu\Omega\hat{\mathbf{H}}^q \tag{8}$$

where μ is the permeability (it is assumed the magnetic conductivity is zero although this is not required). This yields two equations

$$\hat{H}_{x0} = \frac{K_y}{\mu\Omega}\hat{E}_0, \tag{9}$$

$$\hat{H}_{y0} = -\frac{K_x}{\mu\Omega}\hat{E}_0. \tag{10}$$

Using (9) and (10) in (7), one obtains the dispersion equation for lossy media

$$K_x^2 + K_y^2 = \Omega^2\mu\epsilon\left[1 - j\frac{\sigma A}{\epsilon\Omega}\right] \tag{11}$$

This is the dispersion relationship for lossy material which was previously considered in [6] and more recently studied in [7]. We define the complex permittivity to be

$$\hat{\epsilon} = \epsilon\left[1 - j\frac{\sigma A}{\epsilon\Omega}\right] \tag{12}$$

$$= \epsilon\left[1 - jL_\sigma\cot\left(\frac{\omega\Delta_t}{2}\right)\right] \tag{13}$$

where the loss-factor L_σ is defined as $\sigma\Delta_t/(2\epsilon)$, the real quantity ϵ is given by $\epsilon_0\epsilon_r$ and ϵ_0 is the permittivity of free space. Expressed in terms of the underlying functions the dispersion relation is

$$\begin{aligned} \sin^2(\kappa_x) + \sin^2(\kappa_y) = \frac{\mu_r\epsilon_r}{S_c^2}\sin^2\left(\frac{\omega\Delta_t}{2}\right) \\ \times\left[1 - jL_\sigma\cot\left(\frac{\omega\Delta_t}{2}\right)\right] \end{aligned} \tag{14}$$

where κ_ξ is $\tilde{k}_\xi\delta/2$ and $\xi \in \{x, y\}$.

In the construction of the AFP TFSF boundary the frequency and the wave vector components in the first medium can be easily calculated. Due to phase matching along the boundary, the tangential component of the wave number must be the same in both media, i.e., $\tilde{k}_{y2} = \tilde{k}_{y1}$ when the interface corresponds to a constant x plane. We ignore superluminal wave numbers and hence $\tilde{k}_{y2}$ is purely real. (Throughout the analysis we ignore superluminal propagation which is inherently present but of little practical concern. See [8], [9] for further details.) Since the frequency is known, the only unknown in (14) is $\hat{\tilde{k}}_x$, the normal component of the wavenumber which is complex due to the loss. We separate the real and imaginary parts of $\hat{\tilde{k}}_x$ as $\hat{\tilde{k}}_x = \tilde{k}'_x + j\tilde{k}''_x$ or, correspondingly, $\hat{\tilde{k}}_x\delta/2 = \hat{\kappa}_x = \kappa'_x + j\kappa''_x$. Plugging this into (14), expanding terms, and separating real and imaginary parts yields

$$\cos(\kappa'_x)\cosh(\kappa''_x) = C' \tag{15}$$

$$\sin(\kappa'_x)\sinh(\kappa''_x) = C'' \tag{16}$$

where

$$C' = 1 + 2\left[\sin^2(\kappa_y) - \frac{\mu_r\epsilon_r}{S_c^2}\sin^2\left(\frac{\omega\Delta_t}{2}\right)\right] \tag{17}$$

$$C'' = -\frac{\mu_r\epsilon_r}{S_c^2}L_\sigma\sin(\omega\Delta_t). \tag{18}$$

Solving (15) and (16) for κ'_x and κ''_x (and using physical argument to eliminate nonphysical solutions) yields

$$\kappa'_x = \frac{1}{2}\cos^{-1}\left[\frac{UV}{\sqrt{8}C'}\right] \tag{19}$$

$$\kappa''_x = -\frac{1}{2}\cosh^{-1}\left[\frac{U}{\sqrt{2}}\right] \tag{20}$$

where

$$U = \left(M + \sqrt{(M - 2C')(M + 2C')}\right)^{1/2} \tag{21}$$

$$V = M - \sqrt{(M - 2C')(M + 2C')} \tag{22}$$

$$M = 1 + C'^2 + C''^2. \tag{23}$$

The numeric reflection and transmission coefficients for TM^z polarization were presented in [5], [10] for isotropic media and in [3] for uniaxial media. We assume an interface which is aligned with the E_z and H_x nodes as shown in Fig. 1. The FDTD reflection and transmission coefficients which were derived in [5] still pertain to the lossy case—the only difference is that the permittivity and wavenumber in the second medium become complex. When the electric-field nodes on the interface use the arithmetic average of the values to either side for the conductivity and the real part of the permittivity while the magnetic-field nodes on the interface use the harmonic mean for the permeability (i.e., $\mu_a = 2\mu_1\mu_2/(\mu_1 + \mu_2)$), the reflection and transmission coefficients are, respectively

$$\hat{\tilde{\Gamma}}_{tm} = \frac{\mu_2\sin(2\kappa_{1x}) - \mu_1\sin(2\hat{\kappa}_{2x})}{\mu_2\sin(2\kappa_{1x}) + \mu_1\sin(2\hat{\kappa}_{2x})} \tag{24}$$

$$\hat{\tilde{T}}_{tm} = \frac{2\mu_2\sin(2\kappa_{1x})}{\mu_1\sin(2\kappa_{1x}) + \mu_2\sin(2\hat{\kappa}_{2x})}. \tag{25}$$

If one does not use the average material properties at the interface, an additional term appears as was described in [5]. This additional term can cause the agreement between the FDTD and continuous-world values to be better than when using averaging.

However, this improvement only exists over a very narrow band of frequencies and the agreement is worse at all other frequencies. Hence we continue to assume that the mean values are used for the interface material parameters.

The same results pertains to TE^z polarization, i.e., (19) and (20) still pertain. The reflection and transmission coefficients derived in [5] are still pertinent provided one allows the permittivity and wavenumber to be complex. The assumed TE^z grid is shown in Fig. 2. If the arithmetic mean is used for the conductivity and permittivity on the boundary, the reflection and transmission coefficients are [5]

$$\hat{\hat{\Gamma}}_{te} = \frac{\epsilon_1 \sin(\hat{\kappa}_{x2})\cos(\kappa_{x1}) - \hat{\epsilon}_2 \sin(\kappa_{x1})\cos(\hat{\kappa}_{x2})}{\epsilon_1 \sin(\hat{\kappa}_{x2})\cos(\kappa_{x1}) + \hat{\epsilon}_2 \sin(\kappa_{x1})\cos(\hat{\kappa}_{x2})} \quad (26)$$

$$\hat{\hat{T}}_{te} = \frac{2\hat{\epsilon}_2 \sin(\kappa_{x1})\cos(\kappa_{x1})}{\epsilon_1 \sin(\hat{\kappa}_{x2})\cos(\kappa_{x1}) + \hat{\epsilon}_2 \sin(\kappa_{x1})\cos(\hat{\kappa}_{x2})}. \quad (27)$$

Using the wavenumbers as well as the reflection and transmission coefficients described here, the implementation of the AFP TFSF boundary then follows the implementation described in [5].

III. Incidence Beyond the Critical Angle

By allowing the normal component of the wave number in the second medium to be complex, the capability is inherently present to model incoming fields which are incident beyond the critical angle, i.e., the fields are evanescent in the second medium. The critical angle in the FDTD world differs from that in the continuous world [9] and is, in fact, a function of frequency. Nevertheless, we will refer to the critical angle as if it were a constant.

When modeling incidence beyond the critical angle, one must keep in mind the unusual behavior of the incident field. The geometry assumed here is of an infinite, pulsed incoming plane wave propagating obliquely toward an infinite planar interface separating two half spaces in which the speed of propagation in the second medium is faster than in the first. Roughly speaking, fields in the second medium will move tangentially along the boundary faster than they move in the first. However, to satisfy the boundary conditions along the interface, these faster fields will couple energy back into the first medium. These fields will be in advance of the incoming wave. These "advanced fields," despite arriving at any given point before the incoming wave, are causal. A good discussion of these fields can be found in [11], [12].

In theory, the advanced fields are nonzero throughout space and this could be problematic for implementation of a TFSF boundary which assumes the fields are initially zero throughout the computational domain. However, in practice the advanced fields are small and can be made arbitrarily small by delaying the incoming wave. Additionally, if there is loss present in the second medium, this serves to diminish the advanced fields.

The AFP TFSF implementation is oblivious to the advanced field—the same code can be used for all incident angles. To illustrate the case of incidence beyond the critical angle, Fig. 3 shows the magnitude of the H_z field in a TE^z simulation where $\mu_1 = \mu_2 = \mu_0$, $\epsilon_{r1} = 2$, $\epsilon_{r2} = 1$, the incident angle is 60°, and the Courant number S_c is $1/\sqrt{2}$. The computational domain is 180×200 cells, the interface runs vertically through the middle of the grid, and the TFSF boundary is offset 15 cells from the

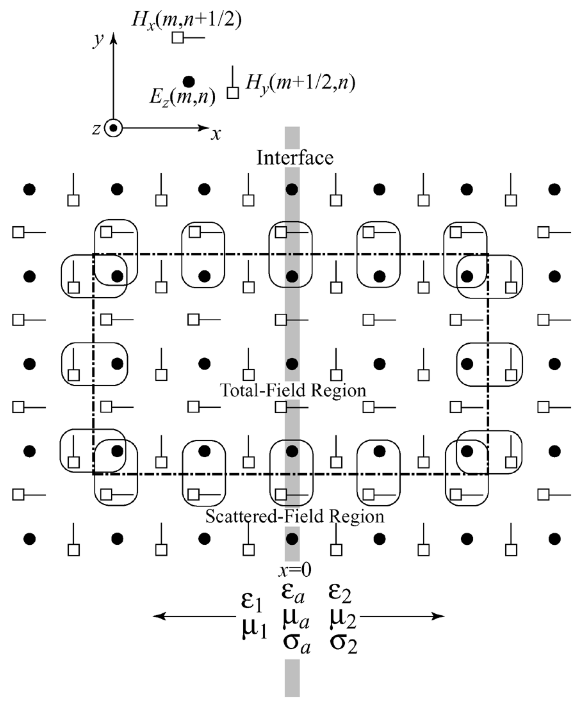

Fig. 1. Depiction of a TM^z grid with two dielectric halfspaces. The interface, corresponding to $x = 0$, is aligned with E_z and H_x nodes. The second medium is assumed lossy. Along the interface the electric-field nodes use the arithmetic average of the permittivity and conductivity to either side while the magnetic-field nodes use the harmonic mean of the permeabilities. The dashed line represents the TFSF boundary. The nodes enclosed in rounded rectangles are tangential to the TFSF boundary and hence must have their updates corrected using the incident field associated with the other node in the box.

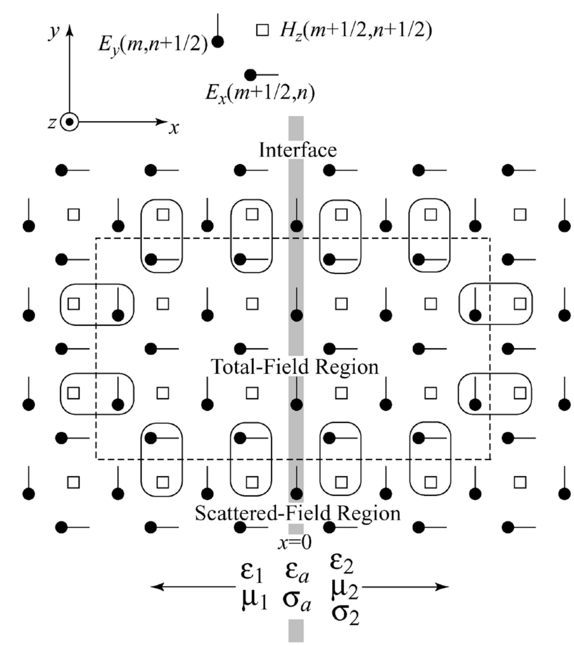

Fig. 2. Depiction of a TE^z grid with two dielectric halfspaces. The interface, corresponding to $x = 0$, is aligned with E_y nodes. For the interface nodes the conductivity and permittivity use the arithmetic mean of the values to either side.

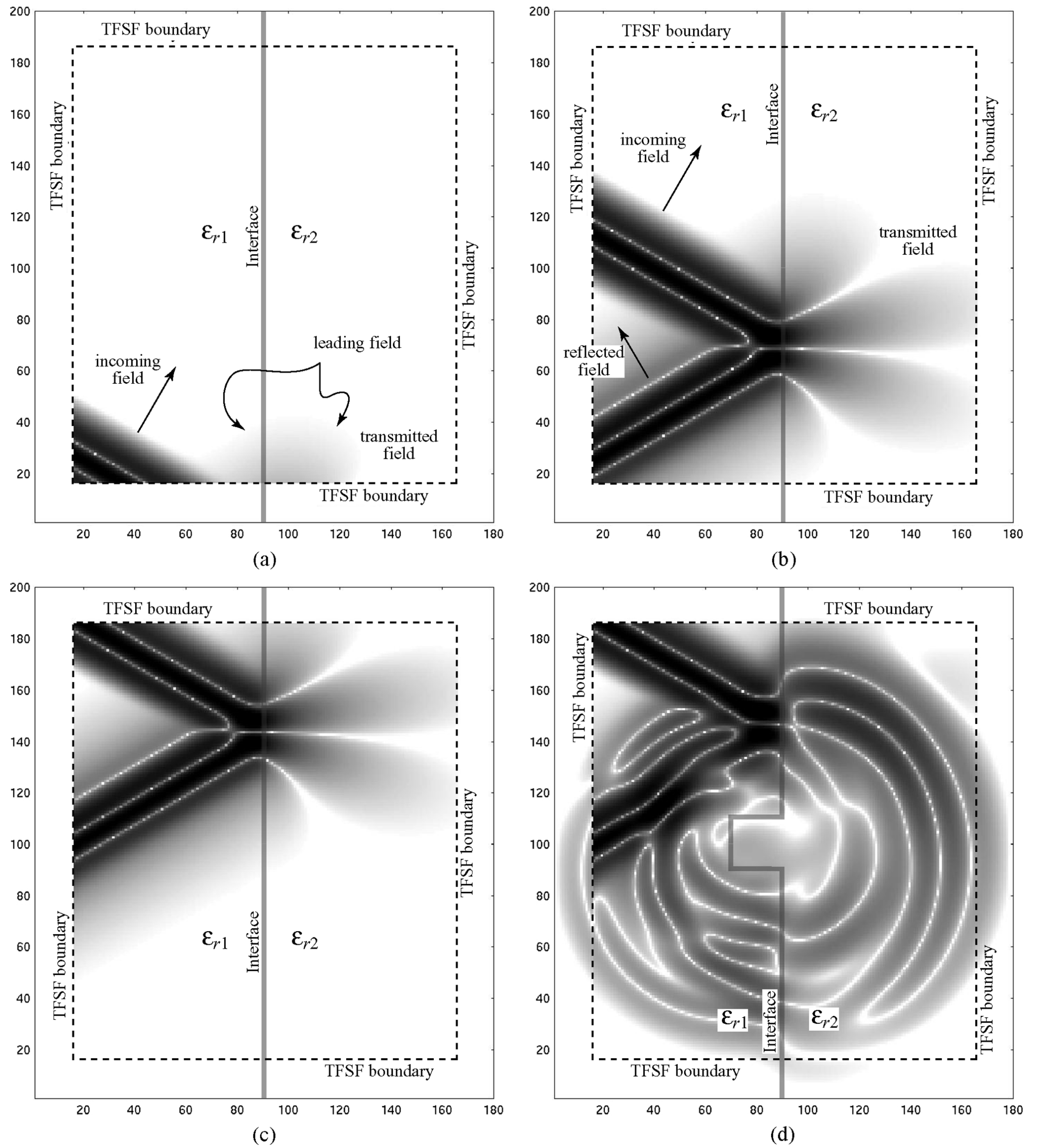

Fig. 3. Snapshots of the magnetic field at time-steps (a) 180, (b) 330, and (c) 460. (d) Magnetic field at time-step 460 showing the field scattered from a notch in the surface. The incident angle is 60° with respect to horizontal.

edge for the grid. The incoming wave is a Ricker wavelet discretized such that there are 20 cells per wavelength (in the first medium) at the frequency with the greatest spectral content.

Fig. 3(a) shows the field at time-step 180. The incoming wave has unit peak amplitude and the images use logarithmic scaling so that fields are essentially visible over three decades. In Fig. 3(a) one can see the distinct incoming field as well as the "haze" associated with the field which arrives in advance of the incoming wave. This leading field exists throughout the computational domain but falls off as one moves away from the incoming wave.

Fig. 3(b) and (c) shows the field at time-steps 330 and 460, respectively. No field is visible in the SF region. For this particular simulation, the peak leaked field is less than 6×10^{-5}. This is much greater than the leaked field found in the typical propagating case where the leaked field is on the order of 10^{-9} for reasonable discretizations. The amount of leaked field can be reduced further by delaying the incoming wave or by changing the source function so that it is has less low-frequency content. Loss in the second medium can also significantly reduce the leaked field.

Fig. 3(d) is also a snapshot at time-step 460. However, to illustrate that the contents of the TF region can be arbitrary, a notch has been placed in the interface. The notch is 20×20 cells where the second medium now protrudes into the first. Because of this notch the fields in the second medium are no longer purely evanescent. One can see the field scattered by the notch and how it has passed into the SF region at this particular time step.

IV. Conclusion

As discussed elsewhere, for problems which can be solved both by the AFP technique and the traditional one-dimensional auxiliary-grid approach, the AFP technique yields far greater accuracy (except in the case of grid-aligned propagation). Furthermore, as demonstrated here, the AFP TFSF technique provides the ability to study many problems which cannot be solved using the traditional one-dimensional (1-D) auxiliary-grid approach. For incident angles beyond the critical angle, the solution obtained from the AFP technique is compromised somewhat by the inherent nature of the field which arrives in advance of the incoming wave. This degradation is unavoidable given the seemingly acausal incident field and it is believed that no other TFSF method could provide better fidelity.

References

[1] D. E. Merewether, R. Fisher, and F. W. Smith, "On implementing a numeric Huygen's source scheme in a finite difference program to illuminate scattering bodies," *IEEE Trans. Nucl. Sci.*, vol. 27, no. 6, pp. 1829–1833, Dec. 1980.

[2] A. Taflove and S. Hagness, *Computational Electrodynamics: The Finite-Difference Time-Domain Method*, 3rd ed. Boston, MA: Artech House, 2005.

[3] C. D. Moss, F. L. Teixeira, and J. A. Kong, "Analysis and compensation of numerical dispersion in the FDTD method for layered, anisotropic media," *IEEE Trans. on Antennas and Propagation*, vol. 50, no. 9, pp. 1174–1184, Sep. 2002.

[4] J. B. Schneider, "Plane waves in FDTD simulations and a nearly perfect total-field/scattered-field boundary," *IEEE Trans. Antennas Propagat.*, vol. 52, no. 12, pp. 3280–3287, Dec. 2004.

[5] J. B. Schneider and K. Abdijalilov, "Analytic field propagation TFSF boundary for FDTD problems involving planar interfaces: PECs, TE, TM ," *IEEE Trans. Antennas Propagat.*, vol. 54, no. 9, pp. 2531–2542, Sep. 2006.

[6] J. A. Pereda, O. García, A. Vegas, and A. Prieto, "Numerical dispersion and stability analysis of the FDTD technique in lossy dielectrics," *IEEE Microw. Guided Wave Lett.*, vol. 8, no. 7, pp. 245–247, Jul. 1998.

[7] G. Sun and C. W. Trueman, "Numerical dispersion and numerical loss in explicit finite-difference time-domain methods in lossy media," *IEEE Trans. Antennas Propagat.*, vol. 53, no. 11, pp. 3684–3690, 2005.

[8] J. B. Schneider and C. L. Wagner, "FDTD dispersion revisited: faster-than-light propagation," *IEEE Microw. Guided Wave Lett.*, vol. 9, no. 2, pp. 54–56, Feb. 1999.

[9] J. B. Schneider and R. J. Kruhlak, "Dispersion of homogeneous and inhomogeneous waves in the Yee finite-difference time-domain grid," *IEEE Trans. Microw. Theory Techn.*, vol. 49, no. 2, pp. 280–287, Feb. 2001.

[10] A. Christ, S. Benkler, J. Frohlich, and N. Kuster, "Analysis of the accuracy of the numerical reflection coefficient of the finite-difference time-domain method at planar material interfaces," *IEEE Trans. Electromagn. Compat.*, vol. 48, no. 2, pp. 264–272, May 2006.

[11] V. L. Brudny and W. L. Mochán, "On the apparent superluminality of evanescent waves," *Opt. Express*, vol. 9, no. 11, pp. 561–566, 2001.

[12] ——, "FTIR and the illusion of superluminality," in *Proc. 2004 OSA Annual Meeting*, Rochester, NY, Oct. 2004.